Hydroxyl radical reaction rate coefficients as a function of temperature and IR absorption cross sections for CF3CH=CH2 (HFO-1243zf), potential replacement of CF3CH2F (HFC-134a)

ARTICLE *in* ENVIRONMENTAL SCIENCE AND POLLUTION RESEARCH · AUGUST 2014

Impact Factor: 2.83 · DOI: 10.1007/s11356-014-3426-2 · Source: PubMed

5 AUTHORS, INCLUDING:

Elena Jiménez
University of Castilla-La Mancha
50 PUBLICATIONS **497** CITATIONS
SEE PROFILE

Bernabé Ballesteros
University of Castilla-La Mancha
33 PUBLICATIONS **358** CITATIONS
SEE PROFILE

Jose Albaladejo
Ferrer Internacional SA
76 PUBLICATIONS **613** CITATIONS
SEE PROFILE

Environ Sci Pollut Res
DOI 10.1007/s11356-014-3426-2

Hydroxyl radical reaction rate coefficients as a function of temperature and IR absorption cross sections for $CF_3CH=CH_2$ (HFO-1243zf), potential replacement of CF_3CH_2F (HFC-134a)

Sergio González · Elena Jiménez · Bernabé Ballesteros · Ernesto Martínez · José Albaladejo

Received: 22 January 2014 / Accepted: 7 August 2014

Abstract $CF_3CH=CH_2$ (hydrofluoroolefin, HFO-1243zf) is a potential replacement of high global-warming potential (GWP) hydrofluorocarbon (HFC-134a, CF_3CFH_2). Both the atmospheric lifetime and the radiative efficiency of HFO-1243zf are parameters needed for estimating the GWP of this species. Therefore, the aim of this work is (i) to estimate the atmospheric lifetime of HFO-1243zf from the reported OH rate coefficients, k_{OH}, determined under tropospheric conditions and (ii) to calculate its radiative efficiency from the reported IR absorption cross sections. The OH rate coefficient at 298 K also allows the estimation of the photochemical ozone creation potential (ε^{POCP}). The pulsed laser photolysis coupled to a laser-induced fluorescence technique was used to determine k_{OH} for the reaction of OH radicals with HFO-1243zf as a function of pressure (50–650 Torr of He) and temperature (263–358 K). Gas-phase IR spectra of HFO-1243zf were recorded at room temperature using a Fourier transform IR spectrometer between 500 and 4,000 cm^{-1}. At all temperatures, k_{OH} did not depend on bath gas concentration (i.e., on the total pressure between 50 and 650 Torr of He). A slight but noticeable T dependence of k_{OH} was observed in the temperature range investigated. The observed behavior is well described by the following Arrhenius expression: $k_{OH}(T)=(7.65\pm0.26)\times10^{-13}$ exp $[(165\pm10)/T]cm^3$ $molecule^{-1}$ s^{-1}. Negligible IR absorption of HFO-1243zf was observed at wavenumbers greater than 1,700 cm^{-1}. Therefore, IR absorption cross sections, $\sigma\widetilde{\nu}$, were determined in the 500–1,700 cm^{-1} range. Integrated $\sigma\widetilde{\nu}$ were determined between 650 and 1,800 cm^{-1} for comparison purposes. The main diurnal removal pathway for HFO-1243zf is the reaction with OH radicals, which accounts for 64 % of the overall loss by homogeneous reactions at 298 K. Globally, the lifetime due to OH reaction (τ_{OH}) was estimated to be 8.7 days under the assumption of a well-mixed atmosphere. Assuming other removal pathways, the atmospheric lifetime (τ) was estimated to be ~6 days. Considering the estimated τ_{OH} and the measured IR absorption cross sections of HFO-1243zf in the atmospheric window (720–1,250 cm^{-1}), its lifetime corrected radiative efficiency was calculated to be 0.019 W m^{-2} $ppbv^{-1}$. $GWP_{100\ years}$ for the HFO investigated, 0.29, is negligible compared to that of HFC-134a, the HFC to be potentially replaced ($GWP_{100\ years}$=1,300, Hodnebrog et al. (Rev Geophys 51:300–378, 2013)). ε_{POCP} for HFO-1243zf was estimated to be around 1 order of magnitude lower than that for ethylene. In conclusion, HFO-1243zf is fast degraded in the atmosphere, and it does not appreciably contribute to global warming and local/regional air pollution. Therefore, HFO-1243zf can be a suitable replacement for HFC-134a in air conditioning units.

Keywords Gas-phase rate coefficients · OH radicals · HFO-1243zf · Lifetime · IR absorption cross sections · Radiative efficiency

Responsible editor: Philippe Garrigues

Electronic supplementary material The online version of this article (doi:10.1007/s11356-014-3426-2) contains supplementary material, which is available to authorized users.

S. González · E. Jiménez · B. Ballesteros · E. Martínez · J. Albaladejo
Department of Physical Chemistry, Faculty of Chemical Sciences and Technologies, University of Castilla–La Mancha, Avda. Camilo José Cela s/n, 13071 Ciudad Real, Spain

E. Jiménez · B. Ballesteros · E. Martínez · J. Albaladejo (✉)
Research Institute on Combustion and Atmospheric Pollution, University of Castilla–La Mancha, Camino de Moledores s/n, 13071 Ciudad Real, Spain
e-mail: Jose.Albaladejo@uclm.es

Introduction

Chlorofluorocarbons (CFCs) are long-lived species in the atmosphere with high ozone depletion potential (ODP) and

Published online: 21 August 2014

high global-warming potential (GWP). Hydrofluorocarbons (HFCs), included in the Kyoto protocol, were considered as good CFC alternatives. HFCs have zero ODP, but they significantly contribute to the greenhouse effect because of the presence of IR absorbing C–F bonds. Hydrofluoroolefins (HFOs), a new generation of HFCs, are currently under consideration as low-GWP alternatives. For instance, 3,3,3-trifluoropropene ($CF_3CH=CH_2$, HFO-1243zf) has been proposed as a replacement for 1,2,2,2-tetrafluoroethane (CF_3CFH_2, HFC-134a) in mobile air conditioning units (USEPA 2010). In the troposphere, HFOs mainly react with the major diurnal tropospheric oxidant, hydroxyl (OH) radicals, but in coastal regions, their degradation initiated by chlorine (Cl) atoms at dawn can become more important.

$$OH + CF_3CH = CH_2 \rightarrow \text{Products} \qquad k_{OH} \qquad (1)$$

Given that reaction 1 proceeds via the OH addition to the double bond of $CF_3CH=CH_2$ (Nakayama et al. 2007), a pressure dependence of k_{OH} is expected to be observed. Reaction 1 was previously investigated by Orkin et al. (1997) and Sulbaek Andersen et al. (2005) at a single pressure. Orkin et al. (1997) reported k_{OH} as a function of temperature (252–370 K) in 100 Torr of Ar, using the flash photolysis–resonance fluorescence (FP–RF) technique. More recently, Sulbaek Andersen et al. (2005) employed the long path length Fourier transform infrared (FTIR)–smog chamber relative technique at 296 K and 700 Torr of N_2 or air to determine k_{OH}, whose value was substantially lower than that reported by Orkin et al. (1997) at 100 Torr of Ar. Within the uncertainty limits reported, it seems that there is no pressure dependence of k_{OH} between 100 and 700 Torr. Nevertheless, there are no experimental evidences that the high pressure limit is reached at lower total pressures than 100 Torr using He as a bath gas, as it was observed for other fluorinated alkenes (Baasandorj et al. 2010; Vésine et al. 2000).

From the theoretical point of view, reaction 1 has been recently investigated using different theoretical methods (Thomsen and Jørgensen 2009; Zhang et al. 2012; Balaganesh and Rajakumar 2014). Thomsen and Jorgensen (2009) reported that computed k_{OH}(298 K) for the addition reaction of OH radical with $CF_3CH=CH_2$ using DFT, MP2, and CCSD(T) methods was in good agreement with experimental values at 298 K. Recently, Zhang et al. (2012) have predicted by multichannel RRKM and transition state theory calculations that k_{OH}(298 K) for reaction 1 was independent of a total pressure between 10 and 10^{10} Torr (of Ar and N_2). However, the temperature dependence of k_{OH} in Ar between 252 and 370 K experimentally observed by Orkin et al. (1997) was not theoretically reproduced by Zhang et al. (2012). More recently, Balaganesh and Rajakumar (2014) performed calculations on k_{OH} for reaction 1 at the MP2 and BMC-CCSD levels of theory in the temperature range of 200–3,000 K in accordance with the T dependence reported by Orkin et al. (1997).

The aim of this work is, therefore, to investigate for the first time the effect of total pressure on k_{OH} for reaction 1 between 50 and 650 Torr of He at several temperatures (263–358 K). The atmospheric lifetime of HFO-1243zf and its photochemical ozone creation potential (POCP) will be estimated from k_{OH}(298 K) derived from the obtained T expression.

In addition to the kinetic measurements, the IR absorption cross sections between 500 and 1,800 cm^{-1} and the radiative efficiency of HFO-1243zf in the atmospheric IR window are also reported at room temperature. The obtained radiative efficiency and the OH rate coefficients allow the estimation of GWP and the evaluation of the atmospheric impact of potential emissions of HFO-1243zf, as a consequence of its use as HFC-134a replacement in air conditioning units.

Experimental

Techniques and methodologies

Two experimental systems have been employed in this study. The first experimental setup is based on the pulsed laser photolysis/laser-induced fluorescence (PLP/LIF) absolute kinetic technique and was employed for determining the OH rate coefficient as a function of temperature and pressure, k_{OH}. The second experimental system, based on Fourier transform infrared (FTIR) spectroscopy, was employed for determining the IR absorption cross sections, $\sigma\tilde{\nu}$, of HFO-1243zf and their integrated values over a specific wavenumber range, S_{int}. The experimental setups, techniques, and methodologies are described in detail in previous works (Jiménez et al. 2007, 2005; 2010; Antiñolo et al. 2010, 2012). Only a brief description is given below.

PLP/LIF technique

This technique has been widely employed by our group to perform gas-phase kinetic studies at temperatures and pressures of atmospheric interest. In this investigation, the PLP/LIF technique was also used to determine the OH rate coefficient for reaction 1.

The reaction cell consists in a jacketed Pyrex reactor with ca. 200 cm^3 of internal volume. The temperature was controlled by a thermostatic bath (JULABO, model FP50), which circulates water ($T \geq 298$ K) or ethanol ($T < 298$ K) through the external jacket of the reactor. A chromel–alumel thermocouple inserted just above the center of the reactor where the reaction takes place was used to monitor the temperature.

A summary of the experimental conditions employed is presented in Table 1. The total pressure, p_T, in the Pyrex

Table 1 Summary of experimental conditions for the OH+$CF_3CH{=}CH_2$ reaction as a function of temperature over the pressure range of 50–650 Torr of He. Stated uncertainties are only statistical errors (95 % level of confidence)

T (K)	p_T (Torr)	$E_{248\ nm}$ (mJ pulse^{-1} cm^{-2})	[$CF_3CH{=}CH_2$] (10^{15} molecules cm^{-3})	[HNO_3][a] (10^{15} molecules cm^{-3})	[H_2O_2][a] (10^{14} molecules cm^{-3})	[OH]$_0$[a] (10^{11} molecules cm^{-3})	$k_{OH}(T)$ (10^{-12} cm^3 molecule^{-1} s^{-1})
263	50	6.78	0.30–1.38	3		5	1.45±0.06
	325	6.48	0.50–1.93	5		8	1.45±0.05
	650	7.09	0.36–1.72	2		3	1.44±0.04
							1.45±0.01
270	50	6.87	0.36–1.42	3		5	1.42±0.04
	325	6.03	0.47–1.81	6		9	1.40±0.06
	650	7.23	0.35–1.68	2		4	1.41±0.02
							1.41±0.02
278	50	6.66	0.33–1.29		4	6	1.39±0.04
	325	7.24	0.40–1.91		2	4	1.37±0.03
	650	8.69	0.47–2.26		3	6	1.38±0.05
							1.38±0.02
287	50	6.13	0.32–1.26		3	5	1.35±0.06
	325	7.16	0.39–1.85		2	4	1.34±0.04
	650	8.83	0.46–2.18		3	6	1.35±0.04
							1.35±0.01
298	50	8.76	0.31–1.21		3	5	1.34±0.05
	140	8.53	0.33–1.56		2	3	1.33±0.06
	220	5.83	0.27–1.08		1	2	1.36±0.05
	325	6.34	0.19–1.17		3	4	1.30±0.05
		7.12	0.31–1.29		4	6	1.15±0.03[b]
	480	5.57	0.24–1.14		2	3	1.35±0.03
	650	8.33	0.45–2.09		2	4	1.32±0.06
							1.31±0.14
308	50	8.24	0.30–1.17		3	6	1.29±0.03
	325	7.09	0.37–1.72		2	3	1.32±0.04
	650	5.40	0.43–2.03		2	2	1.29±0.05
							1.30±0.04
323	50	8.12	0.28–1.12		2	5	1.28±0.05
	325	6.54	0.30–1.43		2	3	1.26±0.04
	650	6.01	0.43–2.01		2	3	1.26±0.04
							1.27±0.02
338	50	6.89	0.13–0.63		2	4	1.26±0.07
		7.32	0.18–0.67		2	4	1.35±0.05[c]
	325	7.57	0.50–1.64		1	3	1.23±0.03
	480	6.47	0.32–1.51		1	2	1.22±0.02
	650	6.14	0.41–1.92		1	2	1.23±0.04

Table 1 (continued)

T (K)	p_T (Torr)	$E_{248\ nm}$ (mJ pulse^{-1} cm^{-2})	[$CF_3CH=CH_2$] (10^{15} molecules cm^{-3})	[HNO_3]^a (10^{15} molecules cm^{-3})	[H_2O_2]^a (10^{14} molecules cm^{-3})	[OH]$_0$^{a} (10^{11} molecules cm^{-3})	$k_{OH}(T)$ (10^{-12} cm^3 molecule^{-1} s^{-1})
							1.26±0.11
358	50	7.74	0.17–0.64		4	7	1.20±0.03
		7.74	0.13–0.59		3	6	1.33±0.07[d]
	325	8.60	0.25–1.15		1	3	1.21±0.06
		8.15	0.31–1.21		1	3	1.17±0.05[e]
	480	5.92	0.29–1.38		2	2	1.20±0.05
	650	7.72	0.32–1.26		1	2	1.20±0.05
							1.22±0.13

The data in italics are the unweighted average rate coefficients

[a] Concentration of the OH precursors and OH radicals are upper limits (see text)

[b] $[O_2]=4.4\times10^{16}$ molecules cm^{-3}

[c] $[O_2]=2.2\times10^{16}$ molecules cm^{-3}

[d] $[O_2]=2.1\times10^{16}$ molecules cm^{-3}

[e] $[O_2]=4.3\times10^{16}$ molecules cm^{-3}

reaction cell ranged from 50 to 650 Torr of He. It was measured by 100- and 1,000-Torr capacitance sensors (Leybold Ceravac CTR90). Diluted mixtures of $CF_3CH=CH_2$ were prepared in 10-L Pyrex bulbs by adding a partial pressure of the HFO, p_{HFO}, and an excess of He, p_{He}. The dilution factor, defined as $f=p_{HFO}/\{p_{HFO}+p_{He}\}$, ranged from 0.3 to 2.2 %. All gases were introduced in the reactor by means of calibrated mass flow controllers. Flow rate ranges were as follows: (i) 1.5–10.3 standard cm^3 per min (sccm) for diluted mixtures of $CF_3CH=CH_2$, F_R (Qualiflow, AFC 50.00); (ii) 0.8–12.7 for He through the glass bubbler containing an aqueous solution of the OH precursor, H_2O_2, or HNO_3 (Qualiflow, AFC 50.00); and (iii) 221–438 sccm for He bath gas (Sierra Instrument Inc., C100L). Thus, total mass flow rates (F_T) were varied from 224 to 461 sccm. The concentrations of HFO-1243zf, [$CF_3CH=CH_2$], inside the reactor were calculated from f value, F_R, F_T, temperature, and pressure. [$CF_3CH=CH_2$] ranged from 1.3×10^{14} to 2.3×10^{15} molecules cm^{-3}.

Ground-state OH radicals, OH($X^2\Pi$), were generated in situ by the pulsed laser photolysis of gaseous H_2O_2 or HNO_3 at 248 nm, an output of a KrF exciplex laser (Optex, Lambda Physik) which was operated at a repetition rate of 10 Hz. Firstly, OH($X^2\Pi$) radicals were pumped to the first electronic excited state, OH($A^2\Sigma^+$), by absorption of radiation at 282 nm. This radiation was generated using a doubled frequency dye laser (Continuum, ND60) pumped by a Nd:YAG laser (Continuum, NY 81 CS-10). A methanolic solution of Rhodamine 6G (dye emission from 546 to 590 nm) was employed to get a radiation of 564 nm, which was subsequently doubled in a doubling unit (Continuum, UVT-1). The energy per pulse, E_λ (mJ/pulse), of probe and photolysis lasers was measured at the entrance of the reactor using a power meter (Ophir, PE50-SH-V2). E_λ for the photolysis laser was varied from 5.40 to 8.83 mJ pulse^{-1}, and for the excitation laser, it was kept below 1 mJ pulse^{-1}. Initial concentrations of OH($X^2\Pi$) ([OH]$_0\leq(2–9)\times10^{11}$ molecules cm^{-3}) were estimated from the OH precursor concentration, [Precursor], and E_λ as described in previous works (Jiménez et al. 2009; Antiñolo et al. 2012, 2014). Upper limits for [Precursor] in the reaction cell were estimated as described by Albaladejo et al. (2002): [H_2O_2]$\leq(1–4)\times10^{14}$ molecules cm^{-3} and [HNO_3]$\leq(2–6)\times10^{15}$ molecules cm^{-3}. Table 1 summarizes the concentration of OH precursor and estimated initial OH concentration for each experiment.

Secondly, the temporal evolution of OH($X^2\Pi$) was monitored by LIF at 308 nm. The OH LIF signal, I_{LIF}, was monitored using a photomultiplier tube (PMT) (Thorn EMI, model 9813B), located at the bottom of the reactor and orthogonally to both laser beams. The LIF signal was focused onto the PMT by means of a plano-convex lens system. A band pass filter (Oriel, BG3) was placed in front of the PMT to minimize the possible interference from other wavelengths. The signal from the PMT was transferred to a computer via a

boxcar integration unit for further analysis. Reaction time (t) was varied by electronically changing the delay between the photolysis and probe lasers. The LIF signal for a given reaction time t, $I_{LIF}(t)$, is proportional to the OH concentration at the same time t.

Kinetic methodology

Loss processes of OH radicals in the reaction cell include reaction with $CF_3CH{=}CH_2$ and OH precursor as well as other losses such as the diffusion out of the detection zone. All experiments were carried out under pseudo-first-order conditions with respect to the initial OH concentration ([$CF_3CH{=}CH_2$] and [Precursor]>>$[OH]_0$). Under these experimental conditions, $I_{LIF}(t)$ is described by a single exponential function corresponding to a pseudo-first-order rate law

$$I_{LIF}(t) = I_{LIF}(t=0)\exp(-k't) \quad (2)$$

where k' is the pseudo-first-order rate coefficient measured in presence or absence (k_0) of $CF_3CH{=}CH_2$. k' and k_0 were obtained from the nonlinear least-squares fit of the LIF decay according to Eq. 2. For a certain temperature and total pressure, k' is given by the following expression:

$$k' = k_{OH}[CF_3CH=CH_2] + k_0. \quad (3)$$

Therefore, k_{OH} was determined from the slope of the plot of k' versus [$CF_3CH{=}CH_2$]. Several plots of Eq. 3, in terms of $k'-k_0$, are shown in Fig. 1 at several temperatures and total pressures. The contributions to k_0 are the OH reaction with the photochemical precursor of OH radicals (k_{prec}) and other OH losses (k_{loss}). Thus, k_0 is given by

$$k_0 = k_{prec}[\text{Precursor}] + k_{loss}. \quad (4)$$

For H_2O_2, the temperature dependence of k_{prec} is that recommended by the Jet Propulsion Laboratory (Sander et al. 2011). k_{prec} for the reaction of OH with HNO_3 was taken from the IUPAC subcommittee on gas kinetic data evaluation (Atkinson et al. 2004). As described by Albaladejo et al. (2002), k_{prec} and k_0 were used to obtain an upper limit for the concentration of H_2O_2 and HNO_3 in the reaction cell and, therefore, an upper limit for the OH initial concentration.

Gas-phase FTIR spectroscopy

The experimental setup employed consists in a FTIR spectrometer (Bruker Tensor 27) coupled to a gas cell of single optical path length (ℓ=10 cm). The cell is built in stainless steel and sealed with ZnSe windows (3.75 cm in diameter). Inside the absorption cell, pressures of diluted mixtures of

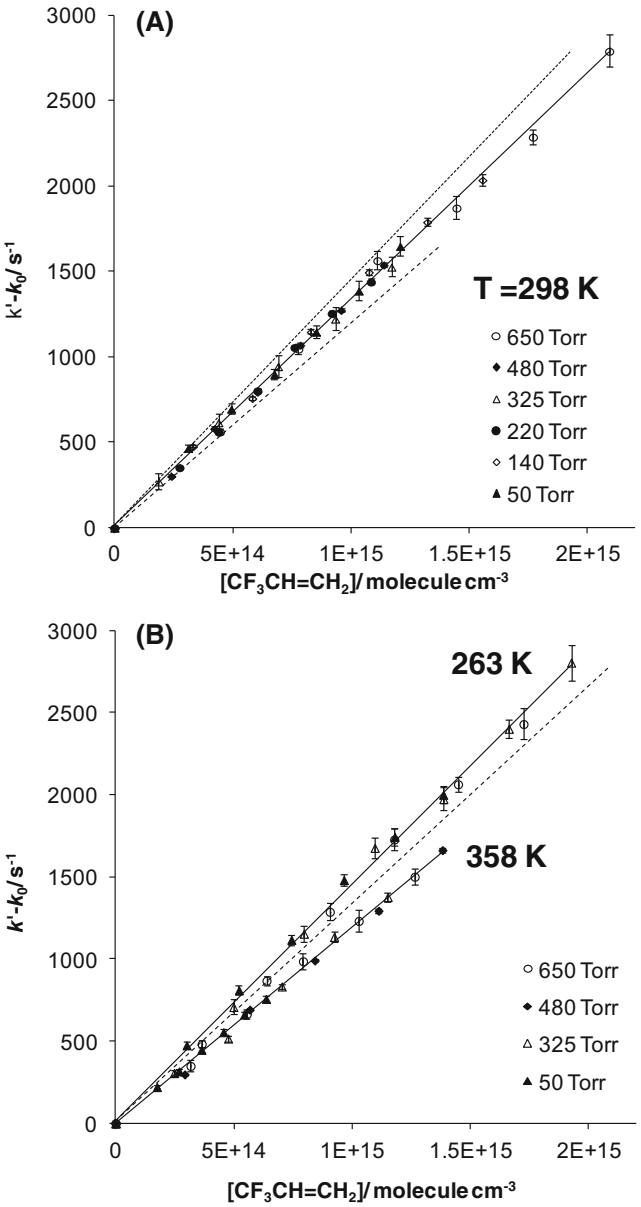

Fig. 1 Plots of $k'-k_0$ versus [$CF_3CH{=}CH_2$] at several total pressures between 50 and 650 Torr and at 298 K (**a**) and at 263 and 358 K (**b**). *Dashed lines* in **a** are the fitting result to data at 263 and 358 K. *Dashed line* in **b** corresponds to the fitting result of data at 298 K

HFO-1243zf in helium (0.6–1.2 %) ranged between 10.5 and 378.5 Torr. The source of infrared radiation is a globular lamp made of silicon carbide which emits between 50 and 6,000 cm^{-1}. A liquid nitrogen-cooled mercury cadmium telluride detector was used for detecting the transmitted IR radiation after passing through the cell (detection range=420–12,000 cm^{-1}). Because of the IR absorption by the ZnSe windows, the detection range was limited to wavenumbers between 500 and 4,000 cm^{-1}. For that reason, IR spectra of HFO-1243zf were recorded at room temperature in that region by coadding 16 interferograms. The spectral resolution in these experiments was set to 1 cm^{-1}. The

absolute IR absorption cross sections, $\sigma\tilde{\nu}$, were obtained by applying the Beer–Lambert law

$$A\tilde{\nu} = \sigma\tilde{\nu}\ell[CF_3CH=CH_2] \quad (5)$$

where $A\tilde{\nu}$ (in base e) is the absorbance at a given wavenumber $\tilde{\nu}$ and $[CF_3CH=CH_2]$ is the hydrofluoroolefin concentration inside the gas cell ($(0.42–7.97)\times10^{16}$ molecules cm^{-3}). $\sigma\tilde{\nu}$ was then determined from the slope of the $A\tilde{\nu}$ versus $[CF_3CH=CH_2]$ plots. Examples of these plots are shown in Fig. S1 of the supporting information for 1,171 cm^{-1} (peak absorption at 1 cm^{-1} resolution) and two other wavenumbers. The Beer–Lambert law is obeyed over the concentration range studied.

The integrated IR absorption cross sections, S_{int}, defined as the integrated $\sigma\tilde{\nu}$ over a specific wavenumber range from $\tilde{\nu}_1$ to $\tilde{\nu}_2$, were obtained by applying the Beer–Lambert law as the same manner as $\sigma\tilde{\nu}$ but using Eq. 5 in terms of the integrated absorbances (A_{int}). In Fig. S2 of the supplementary information, examples of the Beer–Lambert plot (in its integrated form) are presented for the whole measured spectral range (total S_{int}) and several wavenumber ranges between 650 and 1,800 cm^{-1}. S_{int} over 10 cm^{-1} intervals was also determined between 500 and 2,500 cm^{-1} in order to calculate the radiative efficiency of HFO-1243zf (see Calculation of the radiative efficiency and GWP of HFO-1243zf) and to estimate its GWP.

Reagents

Gases Helium from Praxair (99.999 %), O_2 from Carburos Metálicos (99.999 %), and $CF_3CH=CH_2$ from Fluorochem Ltd. (99 %) were employed as supplied.

Solutions Aqueous solution of H_2O_2 (Scharlau, 50 % *w*/*w*) was pre-concentrated prior to use as described elsewhere (Albaladejo et al. 2003). Aqueous solution of HNO_3 (Panreac, 65 %) was used without previous concentration because of the higher vapor pressure of HNO_3 than H_2O.

Results and discussion

Rate coefficients for the OH reaction with HFO-1243zf, k_{OH}

k_{OH} as a function of temperature at several total pressures

As stated in the introduction, k_{OH} was previously reported only at single total pressures, using different bath gases (100 Torr of Ar by Orkin et al. 1997 and 700 Torr of N_2 or air by Sulbaek Andersen et al. 2005). Thus, the present work constitutes the first kinetic study of reaction 1 performed varying the total pressure by more than 1 order of magnitude (p_T=50–650 Torr of He).

The gas-phase rate coefficients for reaction 1 obtained at several total pressures and temperatures between 263 and 358 K are listed in Table 1. Statistical errors in k_{OH} were small (<6 % at 95 % confidence level) and typically ca. 3 % at all temperatures. As can be seen in Table 1 and Fig. 1 as well, no effect of total pressure on k_{OH} was observed in the p_T range investigated. Therefore, an average k_{OH} at each temperature is also reported in Table 1. Conservatively, a systematic uncertainty of ±10 % is considered. This systematic error, which includes uncertainties in the determination of $[CF_3CH=CH_2]$ from flow rates and experimental parameters such as temperature and pressure, can be combined to the statistical uncertainties.

In Table 2, the reported k_{OH} for $CF_3CH=CH_2$ at room temperature is compared with previous kinetic studies and with the OH reactivity of other HFOs. Although Orkin et al. (1997) and Sulbaek Andersen et al. (2005) used different bath gases, k_{OH} is not affected by the different collision efficiency of N_2 (or air) and Ar with respect to He, since the high pressure limit is reached at the investigated total pressures. As shown in Table 2, there is a good agreement between our k_{OH}(298 K) and that of Sulbaek Andersen et al. (2005), within the error limits given. On the other hand, Orkin et al. (1997) found around 15 % higher rate coefficient than ours and that of Sulbaek Andersen et al. (2005). It is worth mentioning that Orkin et al. (1997) only reported statistical errors in k_{OH}.

For the OH reaction with $CH_2=CHF$ and $CH_2=CF_2$, Baasandorj et al. (2010) observed some OH regeneration in the presence of added O_2. These authors found that the measured rate coefficients were systematically lower than the true values, especially at high temperature and low pressure. For reaction 1, the recorded OH profiles at 358 K and 50 Torr were single exponential over two OH lifetimes, indicating a negligible OH regeneration. Nevertheless, in order to confirm that OH regeneration is not the cause of the difference in k_{OH} observed with respect to that of Orkin et al. (1997), some experiments were performed at 50 and 325 Torr for the highest temperature investigated (358 K) in the presence of added O_2 ($(2.1–4.4)\times10^{16}$ molecules cm^{-3}). As it can be observed in Table 1, k_{OH} values obtained in the presence of added O_2 at 298, 338, and 358 K were in concordance with those obtained in the absence of added O_2, within the overall uncertainties.

As it is also shown in Table 2, the reported independence of k_{OH} for reaction 1 with total pressure was also observed, over a similar pressure range to that studied in this work, for other HFOs with one or two F atoms attached to the double bond, such as (E)-$CF_3CH=CHF$, $CF_3CF=CH_2$, and (Z)-$CF_3CF=CHF$ (Orkin et al. 2010; Papadimitriou et al. 2008). The same conclusion was reported for lighter HFOs, such as $CH_2=CF_2$ and $CHF=CH_2$ (Baasandorj et al. 2010), and heavier HFOs, such as $CF_3(CF_2)_3CH=CH_2$ and $CF_3(CF_2)_5CH=CH_2$ (Vésine et al. 2000). Therefore, our results confirm that the high pressure limit of k_{OH} is already reached at

Table 2 Rate coefficients for selected OH+HFO reactions at room temperature

	HFO	p_T (Torr)	k_{OH}(298 K)[a] (10^{-12} cm^3 molecule^{-1} s^{-1})	Reference
C_2	CH_2=CF_2	20–600	2.79±0.25	Baasandorj et al. (2010)
		1–7	2.0±0.4	Howard (1976)
	CHF=CH_2	20–600	5.18±0.50	Baasandorj et al. (2010)
		100	5.56±0.56	Perry et al. (1977)
C_3	CF_3CH=CH_2	50–650	1.31±0.14	This work
		100	1.52±0.02	Orkin et al. (1997)
		700	1.36±0.25	Sulbaek Andersen et al. (2005)
	(Z)-CF_3CF=CHF	25–600	1.29±0.06	Papadimitriou et al. (2008)
	(E)-CF_3CH=CHF	30–200	0.711±0.005	Orkin et al. (2010)
	CF_3CF=CH_2	30–300	1.09±0.02	Orkin et al. (2010)
		25–600	1.12±0.09	Papadimitriou et al. (2008)
C_4	CF_3CF_2CH=CH_2	700	1.36±0.25	Sulbaek Andersen et al. (2005)

[a] Uncertainties are those stated by the authors

50 Torr of He and data from Table 1 can be used for atmospheric modeling.

The temperature dependence of k_{OH} over the T range studied (263–358 K) was observed to be weak, but noticeable (see Fig. 2). As can be seen in Table 1, the difference in k_{OH} between the lowest and the highest temperatures studied is around 16 %. This slight temperature dependence of k_{OH} was well described using the Arrhenius equation, as given by the following expression:

$$k_{OH}(263\text{–}358\ \text{K}) = (7.65 \pm 0.26) \times 10^{-13}\exp\{(165 \pm 10)/T\}\text{cm}^3\ \text{molecule}^{-1}\ \text{s}^{-1}. \quad (6)$$

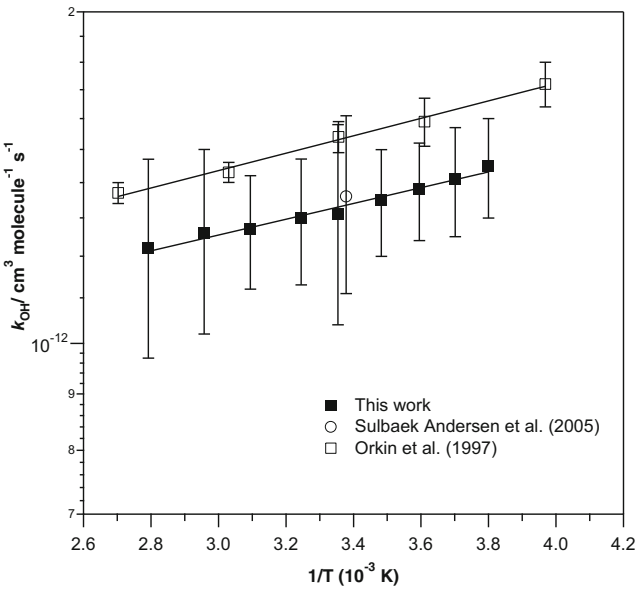

Fig. 2 Arrhenius plot. *Error bars* in this work are the combined statistical and systematic uncertainties

Stated uncertainties are twice the standard deviation derived from the nonlinear regression analysis of the data. The pre-exponential factor, A, and activation energy, E_a, are in good agreement with the previous temperature dependence study on k_{OH} that was carried out by Orkin et al. (1997) between 252 and 370 K at 100 Torr of Ar. The kinetic data reported by these authors have been included in Fig. 2 for comparison with the present measurements. A and E_a/R parameters are listed in Table 3 for reaction 1 together with the Arrhenius parameters obtained by Orkin et al. (1997) and those reported for other selected HFOs. As shown in Table 3, in general, E_a/R values are slightly negative for the selected OH reactions, except for the OH+CF_3CF=CH_2 and $CF_3(CF_2)_5$CH=CH_2 reactions (Orkin et al. 2010; Papadimitriou et al. 2008; Vésine et al. 2000), where a small positive temperature dependence and no dependence were observed, respectively. Furthermore, the kinetic behavior is somewhat different for some of the HFOs and the non-Arrhenius behavior was observed for the OH reactions with (Z)-CF_3CF=CHF (Papadimitriou et al. 2008), (E)-CF_3CH=CHF, and CF_3CF=CH_2 (Orkin et al. 2010). For these reactions, the Arrhenius plots exhibit a curvature and the modified Arrhenius expression, i.e., a T-dependent pre-exponential factor, was preferred (Papadimitriou et al. 2008; Orkin et al. 2010).

Estimation of the tropospheric lifetime (τ) and photochemical ozone creation potential (ε^{POCP}) of HFO-1243zf

Generally, τ is approximated to τ_{OH}, the lifetime due to reaction with the main tropospheric oxidant, i.e., the OH radicals. Nevertheless, a more realistic estimation can be given if other removal pathways are considered (UV photolysis, reaction with other oxidants, deposition, etc.). HFO-1243zf

Table 3 Arrhenius parameters for selected OH+HFO reactions

	HFO	T range (K)	$A\times10^{13}$ (cm^3 molecule^{-1} s^{-1})	E_a/R (K)	Reference
C_2	CH_2=CF_2	220–373	17.5±2.0	−140±20	Baasandorj et al. (2010)
	CHF=CH_2	220–373	17.5±2.0	−316±25	Baasandorj et al. (2010)
		299, 347, 426	14.8	−93±36	Perry et al. (1977)
C_3	CF_3CH=CH_2	263–358	7.65±0.26	−165±10	This work
		252–370	$8.28^{+0.75}_{-0.69}$	−183±26	Orkin et al. (1997)
	(Z)-CF_3CF=CHF	206–380	$(1.6\pm0.2)\times10^{-5}T^2$	−655±50	Papadimitriou et al. (2008)
		200–300	7.3±0.7	−165±20	Papadimitriou et al. (2008)
		220–370	$1.12\times(T/298)^{2.03}$	−552	Orkin et al. (2010)
	CF_3CF=CH_2	220–298	11.5±0.1	+13±3	Orkin et al. (2010)
		298–370	$4.06\times(T/298)^{1.17}$	−296	Orkin et al. (2010)
		206–380	12.6±1.1	+35±10	Papadimitriou et al. (2008)
C_6	$CF_3(CF_2)_3CH$=CH_2	233–372	8.5±1.4	−139±48	Vésine et al. (2000)
C_8	$CF_3(CF_2)_5CH$=CH_2	253–372	13±5	−31±124	Vésine et al. (2000)

Uncertainties are ±2σ

does not absorb the actinic radiation ($\lambda\geq290$ nm), and thus, it is not susceptible to be removed by photolysis (Orkin et al. 1997). There are no data available for heterogeneous reactions neither wet nor dry deposition but are not expected to be important removal pathways for HFO-1243zf. Under these conditions, τ for HFO-1243zf can be obtained from the rate coefficients (k_{Ox}) for its homogeneous reaction with tropospheric oxidants (Ox=OH, NO_3, Cl, or O_3)

$$\tau = \frac{1}{\sum k_{Ox}[Ox]_{24\ h}}. \quad (7)$$

$[Ox]_{24\ h}$ represents the 24-h averaged concentration of the oxidant in the troposphere, as [Ox] may vary significantly with latitude and season. The averaged concentrations are 1×10^6 radicals cm^{-3} for OH radicals (Prinn et al. 2001), 2.5×10^8 molecules cm^{-3} for NO_3 (Finlayson-Pitts and Pitts 2000), 5.3×10^3 atoms cm^{-3} for Cl atoms (Pszenny et al. 1993; Wingenter et al. 1996), and 8.61×10^{11} molecules cm^{-3} for O_3 (Finlayson-Pitts and Pitts 2000).

In the overall tropospheric lifetime of CF_3CH=CH_2, τ is estimated, considering the rate coefficients for the reaction of HFO-1243zf with the main oxidants at 298 K. As k_{OH} was independent of total pressure, Eq. 6 was used to derive the rate coefficient at 298 K, 1.33×10^{-12} cm^3 molecule^{-1} s^{-1}. The rate coefficients for the reaction of HFO-1243zf with Cl atoms (k_{Cl}) and with ozone (k_{O3}) were reported by Sulbaek Andersen et al. (2005) at room T ($k_{Cl}=9.07\times10^{-11}$ cm^3 molecule^{-1} s^{-1} and $k_{O3}=3.05\times10^{-19}$ cm^3 molecule^{-1} s^{-1}). Kinetic studies of reactions of NO_3 radicals with olefinic hydrocarbon compounds are limited. Even though the rate coefficient k_{NO_3} is not available for HFO-1243zf, it should be roughly analogous to that for CF_3CF=CH_2 and (Z)-CF_3CF=CHF (Papadimitriou et al. 2011). These authors reported upper limits for k_{NO_3} of 2.6×10^{-17} and 4.2×10^{-18} cm^3 molecule^{-1} s^{-1} between 233 and 353 K for CF_3CF=CH_2 and (Z)-CF_3CF=CHF, respectively. An upper limit for k_{NO_3} of 10^{-17} cm^3 molecule^{-1} s^{-1} for HFO-1243zf is assumed here. From the individual contributions to τ, it can be deduced that the main removal pathway is the reaction with OH radicals (64 %), followed by the removal initiated by chlorine atoms (23 %) and by ozone (13 %) reactions. The NO_3 reaction is a negligible atmospheric loss process for CF_3CH=CH_2. Considering exclusively the OH reaction, the lifetime of HFO-1243zf (τ_{OH}) was estimated to be 8.7 days under the assumption of a well-mixed atmosphere. Considering all above loss processes in Eq. 7, the overall lifetime for HFO-1243zf is estimated to be ~6 days. This is an extremely short lifetime compared with that of HFC-134a (τ=13.4 years) (WMO 2010). Estimated τ is considered in Calculation of the radiative efficiency and GWP of HFO-1243zf for estimating the GWP of HFO-1243zf.

Another tool for evaluating the impact of an increment in the emission of HFO-1243zf is to estimate the POCP. The POCP method calculates the total additional ozone formed in a multiday modeling of adding a given amount of HFO, in this case, relative to adding the same mass of ethylene (POCP=100). POCP for a specific compound depends upon the model employed in the calculation and other parameters used in its calculation. Derwent et al. (1998) and Jenkin (1998) developed a simplified method which rationalizes POCP values in terms of the structure of the emitted compound (i.e., the molecular weight, the number of carbon atoms, and the number of C–H and C–C bonds) and its OH reactivity at 298 K and 760 Torr. Using the room temperature rate coefficient derived from Eq. 6 ($k_{OH}=1.33\times10^{-12}$ cm^3 molecule^{-1} s^{-1}), for HFO-1243zf, a ε^{POCP} of 10.2 has been calculated, which is

similar to that estimated by Wallington et al. (2010). This value is almost 1 order of magnitude lower than that for ethylene, indicating that its contribution to the photochemical smog will be negligible. Note that the reported ε^{POCP} only considers a part of the overall oxidation processes. As stated by Jenkin (1998), the formation of an unreactive (k_{OH} ~1×10^{-12} cm^3 molecule^{-1} s^{-1}) product in the oxidation of the organic compound leads to greater values of τ^{POCP} with respect to POCP. The introduction of a correction factor in these cases requires a detailed knowledge of the degradation chemistry. For HFO-1243zf, the oxidation products for the OH reaction in the presence of NO_x were investigated by Nakayama et al. (2007). The reaction proceeds via addition to the >C=C< double bond leading to the formation of CF_3CHO in a yield of 88±9 %. CF_3CHO is considered as an unreactive product since the rate coefficient for the OH+CF_3CHO reaction at 298 K is reported to be 5.7×10^{-13} cm^3 molecule^{-1} s^{-1} (Atkinson et al. 2008). Therefore, the POCP for HFO-1243zf is expected to be lower that the estimated ε^{POCP}, confirming that its contribution to the ozone formation in the troposphere will be negligible. To better evaluate the POCP of HFO-1243zf, photochemical trajectory models should include regional emissions (when available), meteorological conditions, chemistry, and non-methane hydrocarbon/NO_x ratios as concluded by Derwent et al. (1996).

Absolute IR absorption cross sections and integrated IR absorption cross sections of HFO-1243zf

Thirty-three IR spectra recorded at several HFO-1243zf concentrations were used to determine $\sigma\widetilde{\nu}$. The resulting averaged IR absorption cross sections (in base *e*) are depicted in Fig. 3a between 500 and 4,000 cm^{-1}. As shown in the figure, strong absorption bands due mainly to absorption by C–F bonds appeared in the 900–1,500 cm^{-1} region (depicted in Fig. 3b). Beyond this region, no significant bands were detected. For that reason, in Online Resource 1, $\sigma\widetilde{\nu}$ values are tabulated in a wavenumber range of 500–1,700 cm^{-1}. The maximum absolute absorption cross section (at 1 cm^{-1} resolution) is observed to be located around 1,171 cm^{-1} and is

$$\sigma_{1{,}171\ \mathrm{cm^{-1}}} = (2.67 \pm 0.11) \times 10^{-18}\ \mathrm{cm^2\ molecule^{-1}}.$$

This result is in fair agreement (around 15 %) with the maximum absorption cross section reported by Sulbaek Andersen et al. (2012) (at 0.25 cm^{-1} resolution), $\sigma_{1{,}170.6\ \mathrm{cm^{-1}}} = 2.31 \times 10^{-18}$ cm^2 molecule^{-1} . Nevertheless, we noticed that the baseline in the IR spectrum of HFO-1243zf reported by Sulbaek Andersen et al. (2012) was shifted downward by 1.6×10^{-20} cm^2 molecule^{-1}. Therefore, $\sigma_{1{,}170.6\ \mathrm{cm^{-1}}}$ can be considered as 2.33×10^{-18} cm^2 molecule^{-1}. This shift affects especially to the integrated absorption cross sections in the 650–1,099 and 1,250–1,800 cm^{-1} regions where the IR absorption is weaker than that for the 1,100–1,249 cm^{-1} band. The integrated absorption cross sections (in base *e*) over 10 cm^{-1} intervals obtained in this work are listed in Online Resource 2. In Fig. S2b of the supporting information, plots of A_{int} versus [$CF_3CH{=}CH_2$] are depicted for the same wavenumber ranges reported by Sulbaek Andersen et al. (2012): 650–1,099, 1,100–1,249, and 1,250–1,800 cm^{-1}. A summary of the obtained S_{int} over the intervals reported by Sulbaek Andersen et al. (2012), after correction of the baseline, is given in Table 4 for comparison purposes. In this work, the total S_{int} was 1.53×10^{-16} cm^2 molecule^{-1} cm^{-1} between 650 and 1,800 cm^{-1}. The difference in S_{int} values with respect to those from Sulbaek Andersen et al. (2012) is less than 11 %, except for S_{int} in the 650–1,099 cm^{-1} region, where the difference is larger. When no baseline correction was applied to the IR spectrum of HFO-1243zf reported by those authors, the difference in total S_{int} was around 23 %.

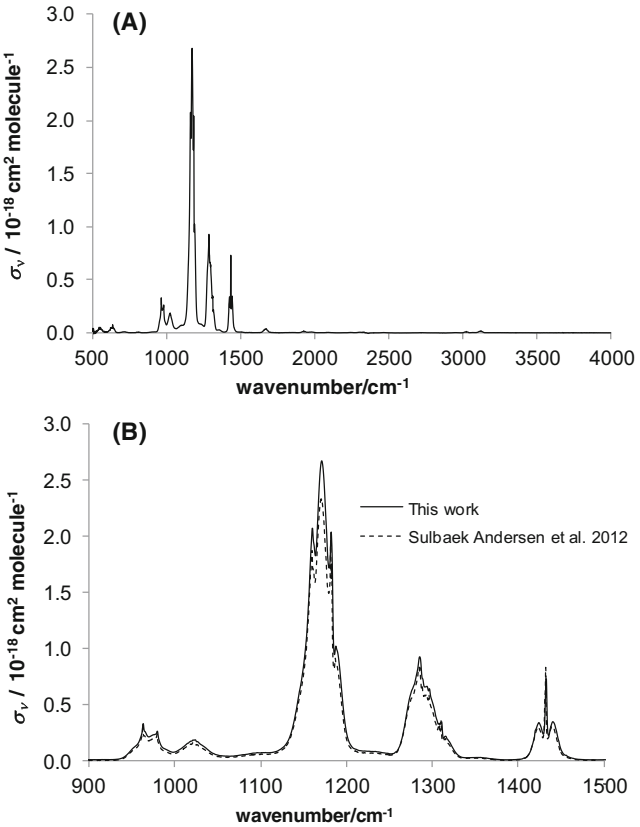

Fig. 3 Absolute IR absorption cross sections of $CF_3CH{=}CH_2$ (in base *e*) determined in this work (**a**) between 500 and 4,000 cm^{-1} (*solid line*). (**b**) Comparison with those reported by Sulbaek Andersen et al. (2012) (*dashed line*)

Calculation of the radiative efficiency and GWP of HFO-1243zf

GWP of a gas *i* is calculated over a time horizon (TH=20, 100, or 500 years) and is based on the time-integrated global

Table 4 Integrated absorption cross sections (base e in 10^{-16} cm^2 molecule^{-1} cm^{-1}) of $CF_3CH{=}CH_2$

Integration wavenumber ranges/cm^{-1}				Reference
650–1,800	650–1,099	1,100–1,249	1,250–1,800	
1.53	0.184	0.904	0.436	This work
1.36	0.155	0.807	0.405	Sulbaek Andersen et al. (2012)

mean radiative forcing (RF) of a pulse emission of 1 kg of the gas relative to that of 1 kg of a reference gas, ref (usually, CO_2) (Forster et al. 2007)

$$\mathrm{GWP}_i(\mathrm{TH}) = \frac{\int_0^{\mathrm{TH}} \mathrm{RF}_i(t)dt}{\int_0^{\mathrm{TH}} \mathrm{RF}_{\mathrm{ref}}(t)dt}. \quad (8)$$

The numerator and denominator of Eq. 8 is the absolute GWP, AGWP(TH), of HFO-1243zf and CO_2, respectively. For HFO-1243zf, AGWP$_i$(TH) (in W m^{-2} year kg^{-1}) can be calculated as follows:

$$\mathrm{AGWP}_i(\mathrm{TH}) = \mathrm{RE}_i\,\tau_i(1-\exp(-\mathrm{TH}/\tau_i)) \quad (9)$$

where RE is the radiative efficiency due to a unit increase in atmospheric abundance of the gas i (in W m^{-2} kg^{-1}) and τ_i (in years) is the atmospheric lifetime for the gas i. Equation 9 assumes that RE is constant over time horizon, and the time-dependent decay in abundance of the gas following an instantaneous release of it at time t=0 obeys a simple exponential decay. It must be noted that the assumption of a simple exponential decay of the atmospheric gas abundance holds for long-lived gases, except for CO_2, but is less accurate for shorter lived gases whose lifetimes depend on location of emissions and physical and chemical conditions of the atmosphere (Hodnebrog et al. 2013). For the reference gas CO_2, the decay of an instantaneous pulse cannot be described by a simple exponential function and AGWP(CO_2) is usually parameterized as (Forster et al. 2007):

$$\mathrm{AGWP}_{\mathrm{CO_2}}(\mathrm{TH}) = \mathrm{RE}_{\mathrm{CO_2}}\left\{a_0\mathrm{TH} + \sum_{i=1}^{3} a_i\alpha_i(1-\exp(-\mathrm{TH}/\alpha_i))\right\} \quad (10)$$

where a_i and α_i (in years) are parameters obtained from the recent multimodel study by Joos et al. (2013) which were used in the most recent review of GWPs (Hodnebrog et al. 2013). AGWP(CO_2) of 9.171×10^{-14} W m^{-2} year(kg CO_2)$^{-1}$ was taken from Hodnebrog et al. (2013) for a time horizon of 100 years.

The instantaneous RE for halocarbons is usually calculated for a 0–1-ppbv increase in mixing ratio (in W m^{-2} ppbv^{-1}). RE$_i$ for HFO-1243zf was calculated by using the narrow-band model by Pinnock et al. (1995) for global and annual mean atmosphere (considering S_{int} from 500 to 2,500 cm^{-1})

$$\mathrm{RE}_i = \sum_{500\ \mathrm{cm^{-1}}}^{2{,}500\ \mathrm{cm^{-1}}} S_{\mathrm{int}}F^{\sigma} \quad (11)$$

where F^{σ} (in W m^{-2}(cm^{-1})$^{-1}$(cm^2 molecule^{-1})$^{-1}$) is the radiative efficiency per absorption cross-section unit parameterized in 10 cm^{-1} intervals. The instantaneous RE for HFO-1243zf was calculated to be 0.21 W m^{-2} ppbv^{-1}. The only available RE value is that reported by Sulbaek Andersen et al. (2012), 0.159 W m^{-2} ppbv^{-1} between 650 and 2,000 cm^{-1}. After the baseline correction, this RE value is slightly higher, 0.18 W m^{-2} ppbv^{-1}. Therefore, the instantaneous RE reported by Sulbaek Andersen et al. (2012) is only 0.02 lower that that obtained from our results in the same wavenumber range (0.20 W m^{-2} ppbv^{-1}).

As discussed by Hodnebrog et al. (2013), one of the largest sources of uncertainty in RE estimates is the effect of a nonuniform vertical profile and geographic distribution of the halocarbon due to their reactivity toward OH in the troposphere (~20 % for compounds with lifetimes shorter than 5 years). To account for this effect, RE$_i$ for HFO-1243zf was corrected by taken into account the fractional correction factor $f(\tau)$ that primarily depends on the atmospheric lifetime

$$f(\tau) = \frac{2.962\tau^{0.9312}}{1+2.994\tau^{0.9302}}. \quad (12)$$

For HFO-1243zf, τ assuming only OH reaction, as used by Hodnebrog et al. (2013), is estimated to be 0.024 years (~8.7 days); therefore, $f(\tau)$ is 0.084. Applying this correction to the resulting instantaneous RE$_i$ from Eq. 11 (0.21 W m^{-2} ppbv^{-1}), the corrected lifetime RE$_i$ is reported to be 0.019 W m^{-2} ppbv^{-1}, which is in good agreement with the value reported by Hodnebrog et al. (2013). It must be noted that Eq. 12 was derived from a 3-D model under the assumption that HFCs only react with OH radicals, which certainly overestimates the lifetime correction and, therefore, the value of GWP.

RE alone cannot be used to assess the potential climate change associated with emissions, as it does not take into

account the different atmospheric lifetimes of the forcing agents. GWP is the parameter that assesses these emissions. Globally averaged GWPs have been calculated for many short-lived species as a comparative index. However, there are serious limitations to the use of global mean GWPs for this purpose (IPCC 2001). While the GWP of the long-lived greenhouse gases (GHGs) do not depend on location and time of emissions, the GWP for short-lived species will be regionally and temporally dependent. In the absence of a metric to assess the possible climate impacts of short-lived species and to compare those with the impacts of the long-lived GHGs, GWP was used for this purpose. Using Eqs. 8–10, GWP for HFO-1243zf is calculated to be 0.29 for a time horizon of 100 years. In spite of the strong absorption of HFO-1243zf in the atmospheric IR window (720–1,250 cm^{-1}), its contribution to the global warming of the Earth is insignificant due to its short lifetime. Therefore, the radiative forcing of climate change of HFO-1243zf is negligible compared to that of HFC-134a, a refrigerant to be replaced ($GWP_{100\ years}$=1,300, Hodnebrog et al. 2013).

Conclusions

In the present work, the experimental determination of $k_{OH}(T=263–358\ K)$ in the 50–650-Torr range is reported. The novelty of the present kinetic study is the experimental confirmation that k_{OH} is independent of total pressure at gas densities of the troposphere. The Arrhenius expression that describes the observed temperature dependence of $k_{OH}(T)$ is provided for being used in modeling of atmospheric chemical processes. As expected, the presence of a C–C double bond in the potential replacement of HFC-134a increases its reactivity toward OH radicals, resulting in a much shorter tropospheric lifetime. The estimated global tropospheric lifetimes for HFO-1243zf (~6 days) imply that this hydrofluoroolefin is fast degraded in the troposphere, limiting its accumulation and minimizing its direct GWP.

The gas-phase oxidation of $CF_3CH=CH_2$ initiated by OH radicals as well as Cl atoms (Nakayama et al. 2007) and O_3 (Sulbaek Andersen et al. 2005) was reported to occur via addition to the double bond. The primary atmospheric oxidation product of the OH and Cl reaction is CF_3CHO (88±9 %) and $CF_3C(O)CH_2Cl$ (70±5 %), respectively (Nakayama et al. 2007). In the presence of NO_x, by analogy with heavier fluoroalkenes, $C_4F_9CH=CH_2$ and $C_6F_{13}CH=CH_2$ (Vésine et al. 2000), $CF_3CH=CH_2$ could be a small source of harmful species like PAN-type compounds. The estimated photochemical ozone creation potential for HFO-1243zf demonstrates that its contribution to the formation of ground ozone is negligible. To better evaluate the POCP of HFO-1243zf, photochemical trajectory models are desirable, whenever information about regional emissions is available.

In conclusion, from the kinetic point of view, $CF_3CH=CH_2$ seems to be a suitable replacement for HFC-134a in mobile air conditioning units. Certainly, the suitability of an HFC replacement candidate is not only based on the GWP parameter. Other selection criteria have to be considered before their widespread use such as their physical properties (e.g., flammability, boiling point, etc.) and their biological and toxicological activity.

Acknowledgments This work has been supported by the Spanish Ministry of Science and Innovation under the project no. CGL2010-19066. The authors would like to thank the reviewers of this work and Claus J. Nielsen for their helpful discussions that have improved this article.

Supporting information Online resources 1 and 2 list $\sigma\widetilde{\nu}$ in the wavenumber range of 500–1,700 cm^{-1} and S_{int} over 10 cm^{-1} intervals between 500 and 2,500 cm^{-1}, respectively. Figure S1 shows the Beer–Lambert law plots for the absorption peak (1,171 cm^{-1}) and other selected wavenumbers. In Fig. S2, some examples of the Beer–Lambert plot (in its integrated form) are presented for the total S_{int} and several wavenumber ranges.

References

Albaladejo J, Ballesteros B, Jiménez E, Martín P, Martínez E (2002) A PLP–LIF kinetic study of the atmospheric reactivity of a series of C_4–C_7 saturated and unsaturated aliphatic aldehydes with OH. Atmos Environ 36:3231–3239. doi:10.1016/S1352-2310(02)00323-0

Albaladejo J, Ballesteros B, Jiménez E, de Mera YD, Martinez E (2003) Gas-phase OH radical-initiated oxidation of the 3-halopropenes studied by PLP-LIF in the temperature range 228–388 K. Atmos Environ 37:2919–2926. doi:10.1016/S1352-2310(03)00297-8

Antiñolo M, Jiménez E, Notario A, Martínez E, Albaladejo J (2010) Tropospheric photooxidation of CF_3CH_2CHO and $CF_3(CH_2)_2CHO$ initiated by Cl atoms and OH radicals. Atmos Chem Phys 10:1911–1922. doi:10.5194/acp-10-1911-2010

Antiñolo M, González S, Ballesteros B, Jiménez E, Albaladejo J (2012) Laboratory studies of $CHF_2CF_2CH_2OH$ and $CF_3CF_2CH_2OH$: UV and IR absorption cross sections and OH rate coefficients between 263 and 358 K. J Phys Chem A 116:6041–6050. doi:10.1021/jp2111633

Antiñolo M, Jiménez E, González S, Albaladejo J (2014) Atmospheric chemistry of CF_3CF_2CHO: absorption cross sections in the UV and IR regions, photolysis at 308 nm, and gas-phase reaction with OH radicals (T=263–358 K). J Phys Chem A 118:178–186. doi:10.1021/jp410283v

Atkinson R, Baulch DL, Cox RA, Crowley JN, Hampson RF, Hynes RG, Jenkin ME, Rossi MJ, Troe J (2004) Evaluated kinetic and photochemical data for atmospheric chemistry: volume I—gas phase reactions of O_x, HO_x, NO_x and SO_x species. Atmos Chem Phys 4:1461–1738. doi:10.5194/acp-4-1461-2004

Atkinson R, Baulch DL, Cox RA, Crowley JN, Hampson RF, Hynes RG, Jenkin ME, Rossi MJ, Troe J, Wallington TJ (2008) Evaluated kinetic and photochemical data for atmospheric chemistry: volume IV—gas phase reactions of organic halogen species. Atmos Chem Phys 8:4141–4496

Baasandorj M, Knight G, Papadimitriou VC, Talukdar RK, Ravishankara AR, Burkholder JB (2010) Rate coefficients for the gas-phase reaction of the hydroxyl radicals with CH_2=CHF and CH_2=CF_2. J Phys Chem A 114:4619–4633. doi:10.1021/jp100527z

Balaganesh M, Rajakumar B (2014) Mechanism, kinetics and atmospheric fate of CF_3CH=CH_2, CF_3CF=CH_2, and CF_3CF=CF_2 by its reaction with OH-radicals: CVT/SCT/ISPE and hybrid meta-DFT methods. J Mol Graph Model 48:60–69. doi:10.1016/j.jmgm.2013.12.003

Derwent RG, Jenkin ME, Saunders SM (1996) Photochemical ozone creation potentials for a large number of reactive hydrocarbons under European conditions. Atmos Environ 30:181–199. doi:10.1016/1352-2310(95)00303-G

Derwent RG, Jenkin ME, Saunders SM, Pilling MJ (1998) Photochemical ozone creation potentials for organic compounds in Northwest Europe calculated with a master chemical mechanism. Atmos Environ 32:2429–2441. doi:10.1016/S1352-2310(98)00053-3

Finlayson-Pitts BJ, Pitts JN (2000) Chemistry of the upper and lower atmosphere. Academic, London

Forster P, Ramaswamy V, Artaxo P, Berntsen T, Betts R, Fahey D W, Haywood J, Lean J, Lowe D C, Myhre G, Nganga J, Prinn R, Raga G, Schulz M, Van Dorland R (2007) Changes in atmospheric constituents and in radiative forcing. In: Solomon S, Qin D, M. Manning, Z. Chen, M. Marquis, K.B. Averyt, M. Tignor and H.L. Miller (eds) Climate change 2007: the physical science basis. Contribution of Working Group I to the Fourth Assessment Report of the Intergovernmental Panel on Climate Change. Cambridge University Press, Cambridge

Hodnebrog Ø, Etminan M, Fuglestvedt JS, Marston G, Myhre G, Nielsen CJ, Shine KP, Wallington TJ (2013) Global warming potentials and radiative efficiencies of halocarbons and related compounds: a comprehensive review. Rev Geophys 51:300–378. doi:10.1002/rog.20013

Howard CJ (1976) Rate constants for the gas-phase reactions of OH radicals with ethylene and halogenated ethylene compounds. J Chem Phys 65:4771–4777. doi:10.1063/1.432932

IPCC (2001) Third assessment report of the International Panel on Climate Change

Jenkin, M E (1998) Photochemical ozone and PAN creation potentials: rationalisation and methods of estimation. AEA Technology pic, Report AEAT-41820/20150/003. AEA Technology pic. National Environmental Technology Centre, Culham

Jiménez E, Ballesteros B, Martínez E, Albaladejo J (2005) Tropospheric reaction of OH with selected linear ketones: kinetic studies between 228 and 405 K. Environ Sci Technol 39:814–820. doi:10.1021/es049333c

Jiménez E, Lanza B, Martínez E, Albaladejo J (2007) Daytime tropospheric loss of hexenal and *trans*-2-hexenal: OH kinetics and UV photolysis. Atmos Chem Phys 7:1565–1574. doi:10.5194/acp-7-1565-2007

Jiménez E, Lanza B, Antiñolo M, Albaladejo J (2009) Influence of temperature on the chemical removal of 3-methylbutanal, *trans*-2-methyl-2-butenal, and 3-methyl-2-butenal by OH radicals in the troposphere. Atmos Environ 43:4043–4049. doi:10.1016/j.atmosenv.2009.05.005

Jiménez E, Antiñolo M, Ballesteros B, Martínez E, Albaladejo J (2010) Atmospheric lifetimes and global warming potentials of $CF_3CH_2CH_2OH$ and $CF_3(CH_2)_2CH_2OH$. Chem Phys Chem 11:4079–4087. doi:10.1002/cphc.201000365

Joos F, Roth R, Fuglestvedt JS (2013) Carbon dioxide and climate impulse response functions for the computation of greenhouse gas metrics: a multi-model analysis. Atmos Chem Phys 13:2793–2825. doi:10.5194/acp-13-2793-2013

Nakayama T, Takahashi K, Matsumi Y, Toft A, Sulbaek Andersen MP, Nielsen OJ, Waterland RL, Buck RC, Hurley MD, Wallington TJ (2007) Atmospheric chemistry of CF_3CH=CH_2 and C_4F_9CH=CH_2: products of the gas-phase reactions with Cl atoms and OH radicals. J Phys Chem A 111:909–915. doi:10.1021/jp0667361

Orkin VL, Huie RE, Kurylo MJ (1997) Rate constants for the reactions of OH with HFC-245cb ($CH_3CF_2CF_3$) and some fluoroalkenes (CH_2CHCF_3, CH_2CFCF_3, CF_2CFCF_3, and CF_2CF_2). J Phys Chem A 101:9118–9124. doi:10.1021/jp971994r

Orkin VL, Martynova LE, Ilichev AN (2010) High-accuracy measurements of OH reaction rate constants and IR absorption spectra: CH_2=CF-CF_3 and *trans*-CHF=CH-CF_3. J Phys Chem A 114:5967–5979. doi:10.1021/jp9092817

Papadimitriou VC, Talukdar RK, Portmann RW, Ravishankara AR, Burkholder JB (2008) CF_3CF=CH_2 and (*Z*)-CF_3CF=CHF: temperature dependent OH rate coefficients and global warming potentials. Phys Chem Chem Phys 10:808–820. doi:10.1039/b714382f

Papadimitriou VC, Lazarou YG, Talukdar RK, Burkholder JB (2011) Atmospheric chemistry of CF_3CF=CH_2 and (*Z*)-CF_3CF=CHF: Cl and NO_3 rate coefficients, Cl reaction product yields, and thermochemical calculations. J Phys Chem A 115:167–181. doi:10.1021/jp110021u

Perry RA, Atkinson R, Pitts JN Jr (1977) Rate constants for the reaction of OH radicals with CH_2=CHF, CH_2=CHCl, and CH_2=CHBr over the temperature range 299–426 K. J Chem Phys 67:458–462. doi:10.1063/1.434889

Pinnock S, Hurley MD, Shine KP, Wallington TJ, Smyth TJ (1995) Radiative forcing of climate by hydrochlorofluorocarbons and hydrofluorocarbons. J Geophys Res 100:23227–23238. doi:10.1029/95JD02323

Prinn RG, Huang J, Weiss RF, Cunnold DM, Fraser PJ, Simmonds PG, McCulloch A, Harth C, Salameh P, O'Doherty S, Wang RHJ, Porter L, Miller BR (2001) Evidence for substantial variations of atmospheric hydroxyl radicals in the past two decades. Science 292:1882–1888. doi:10.1126/science. 1058673

Pszenny AAP, Keene WC, Jacob DJ, Fan S, Maben JR, Zetwo MP, Springer-Young M, Galloway JN (1993) Evidence of inorganic chlorine gases other than hydrogen chloride in marine surface air. Geophys Res Lett 20:699–702. doi:10.1029/93GL00047

Sander SP, Abbatt J, Barker JR, Burkholder JB, Friedl RR, Golden DM, Huie RE, Kolb CE, Kurylo MJ, Moortgat GK, Orkin V, Wine PH (2011) "Chemical kinetics and photochemical data for use in atmospheric studies. Evaluation No. 17," JPL Publication 10-6, Jet Propulsion Laboratory, Pasadena, http://jpldataeval.jpl.nasa.gov

Sulbaek Andersen MP, Nielsen OJ, Toft A, Nakayama T, Matsumi Y, Waterland RL, Buck RC, Hurley MD, Wallington TJ (2005) Atmospheric chemistry of $C_xF_{2x+1}CH$=CH_2 (x=1, 2, 4, 6, and 8): kinetics of gas-phase reactions with Cl atoms, OH radicals, and O_3. J Photochem Photobiol A Chem 176:124–128. doi:10.1016/j.jphotochem.2005.06.015

Sulbaek Andersen MP, Waterland RL, Sander SP, Nielsen OJ, Wallington TJ (2012) Atmospheric chemistry of $C_xF_{2x+1}CH$=CH_2 (x=1, 2, 4, 6 and 8): radiative efficiencies and global warming potentials. J Photochem Photobiol A Chem 233:50–52. doi:10.1016/j.jphotochem.2012.02.020

Thomsen DL, Jørgensen SA (2009) A theoretical study of the kinetics of OH radical addition to halogen substituted propenes. Chem Phys Lett 481:29–33. doi:10.1016/j.cplett.2009.09.026

USEPA (2010) Transitioning to low-GWP alternatives in MVACs. United States Environmental Protection Agency. http://www.epa.gov/ozone/downloads/EPA_HFC_MVAC.pdf

Vésine E, Bossoutrot V, Mellouki A, Le Bras G, Wenger J, Sidebottom H (2000) Kinetic and mechanistic study of OH- and Cl-initiated oxidation of two unsaturated HFCs: C_4F_9CH=CH_2 and $C_6F_{13}CH$=CH_2. J Phys Chem A 104:8512–8520. doi:10.1021/jp0013199

Wallington TJ, Sulbaek Andersen MP, Nielsen OJ (2010) Estimated photochemical ozone creation potentials (POCPs) of CF_3CF=CH_2

(HFO-1234yf) and related hydrofluoroolefins (HFOs). Atmos Environ 44:1478–1481. doi:10.1016/j.atmosenv.2010.01.040

Wingenter OW, Kubo MK, Blake NJ, Smith TW, Blake DR, Rowland FS (1996) Hydrocarbon and halocarbon measurements as photochemical and dynamical indicators of atmospheric hydroxyl, atomic chlorine, and vertical mixing obtained during Lagrangian flights. J Geophys Res 101:4331–4340. doi:10.1029/95JD02457

WMO (2010) Scientific assessment of ozone depletion: 2010. World Meteorological Organization. http://www.esrl.noaa.gov/csd/assessments/ozone/2010/report.html

Zhang Y, Sun J, Chao K, Sun H, Wang F, Tang S, Pan X, Zhang J, Wang R (2012) Mechanistic and kinetic study of $CF_3CH=CH_2+OH$ reaction. J Phys Chem A 116:3172–3181. doi:10.1021/jp209960c